NANO LETTERS

Letter

pubs.acs.org/NanoLett

# Advanced Sulfur Cathode Enabled by Highly Crumpled Nitrogen-Doped Graphene Sheets for High-Energy-Density Lithium–Sulfur Batteries

Jiangxuan Song, Zhaoxin Yu, Mikhail L. Gordin, and Donghai Wang*

Department of Mechanical and Nuclear Engineering, The Pennsylvania State University, University Park, Pennsylvania 16802, United States

Supporting Information

**ABSTRACT:** Herein, we report a synthesis of highly crumpled nitrogen-doped graphene sheets with ultrahigh pore volume (5.4 $cm^3/g$) via a simple thermally induced expansion strategy in absence of any templates. The wrinkled graphene sheets are interwoven rather than stacked, enabling rich nitrogen-containing active sites. Benefiting from the unique pore structure and nitrogen-doping induced strong polysulfide adsorption ability, lithium–sulfur battery cells using these wrinkled graphene sheets as both sulfur host and interlayer achieved a high capacity of ~1000 mAh/g and exceptional cycling stability even at high sulfur content (≥80 wt %) and sulfur loading (5 mg sulfur/$cm^2$). The high specific capacity together with the high sulfur loading push the areal capacity of sulfur cathodes to ~5 mAh/$cm^2$, which is outstanding compared to other recently developed sulfur cathodes and ideal for practical applications.

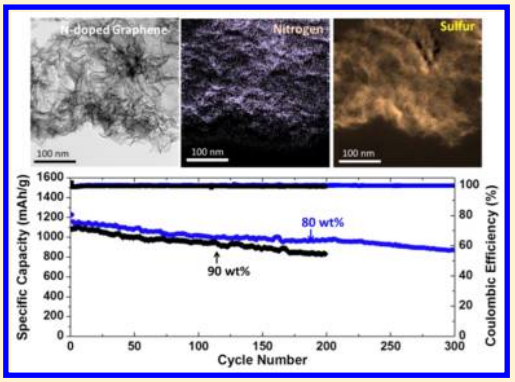


**KEYWORDS:** *Lithium–sulfur batteries, nitrogen-doped graphene, crumpled graphene, high sulfur content, high areal capacity*

Lithium-sulfur (Li–S) batteries are being pursued as the next generation rechargeable battery due to their high theoretical energy density (2600 Wh/kg) and low cost.[1−9] However, practical applications of Li–S batteries are highly hindered by the low electrical conductivity of sulfur and the diffusion of soluble lithium polysulfides intermediates generated during cycling, which lead to lower utilization of sulfur, loss of active material from the cathode, and polysulfide shuttle phenomenon.[10−13] As a result, Li–S cells experience a fast capacity fading, low Coulombic efficiency, and poor rate capability. To address these issues, various types of cathode materials, including porous carbon–sulfur,[14−18] low-dimensional conducting material (such as carbon nanotube[19,20] and graphene[6,7,21])–sulfur, and conducting polymer–sulfur composites, have been exploited to improve the overall electrochemical performance of the Li–S cells. Despite the promising advances, the preparation of sulfur cathodes with long-cycle-life and high Coulombic efficiency still presents challenges, especially for the cathodes with high sulfur content in the cathode and high areal sulfur loading in the electrode, which is necessary toward high-energy-density Li–S battery.[22−24]

Recently, nitrogen-doping of carbon has been demonstrated to be an effective approach for improving the overall electrochemical performance of sulfur cathodes in Li–S batteries.[24−29] Nitrogen-doping, first, can promote chemical bonding between carbon scaffold and sulfur chains upon heat treatment during the sulfur loading process.[24] Second, it can also greatly enhance the adsorption of soluble lithium polysulfides intermediates.[25] The former characteristic helps enable uniform distribution of sulfur in the carbon host initially as well as after redeposition, improving cycling performance; the latter one can effectively retard the diffusion of the lithium polysulfides and trap them within the cathode, thus improving both cycling stability and Coulombic efficiency. Importantly, in contrast to widely used nonconductive adsorbents,[30−33] nitrogen-doped carbon is highly conductive and thus allows for direct redox and utilization of adsorbed material rather than requiring desorption and diffusion of polysulfides to an electrochemically active surface.[25] This unique chemical adsorption ability of both sulfur and polysulfides on nitrogen-doped carbon is attributed to functional groups on the carbon surface induced by nitrogen doping, in which the spin density and charge distribution of carbon atoms will be influenced by the neighbor nitrogen dopants. This kind of functional group can participate in chemisorption directly on conductive carbon surface, thus offering great technological promise for Li–S batteries.[24−28]

Nanoporous structure in carbon has been commonly adopted to host sulfur within the pores, and to maintain the sulfur nanosized and intimate contact with the conductive carbon matrix and thus enhance redox kinetics of the carbon–sulfur composite cathodes. High pore volume and high surface area of the carbon are required to keep high content sulfur

**Received:** August 12, 2015
**Revised:** December 22, 2015
**Published:** December 28, 2015





DOI: 10.1021/acs.nanolett.5b03217
*Nano Lett.* 2016, 16, 864–870

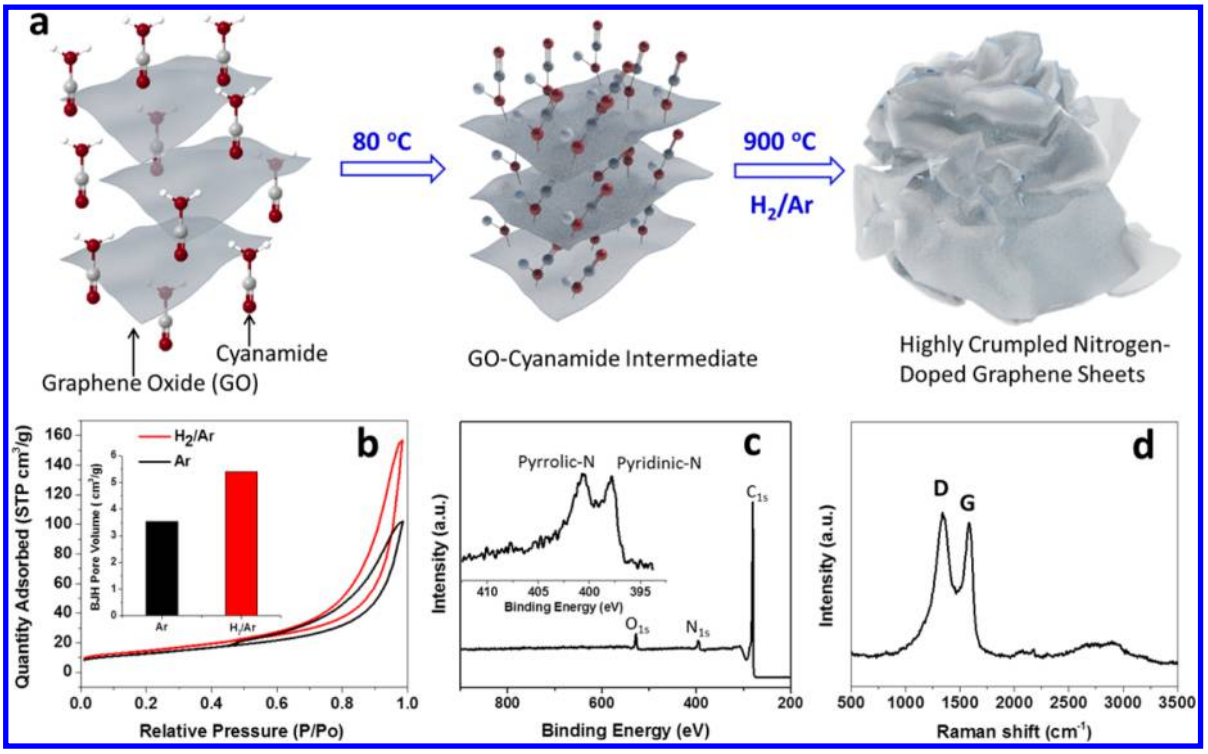


**Figure 1.** (a) Schematic illustration of the synthesis of highly crumpled NG sheets; (b) $N_2$ adsorption/desorption isotherm and BJH pore volume (inset) of the highly crumpled NG sheets with different flow gas during thermal treatment process; (c) XPS survey and $N_{1s}$ detailed spectra (inset) and (d) Raman spectrum of the crumpled NG sheets.

within pore structure. For example, pore volume as high as 5 $cm^3/g$ is minimally needed to accommodate 90% sulfur within pores in the carbon−sulfur composite (see calculation in Table S1 in Supporting Information). Because of the limited pore volume of current nanoporous nitrogen-doped carbon, the sulfur cathodes reported so far have a relatively low sulfur content (≤70 wt %) and sulfur loading (2 mg sulfur/$cm^2$). That is far from practical application, in which high sulfur content (>70 wt %) and sulfur loading (>5 mg sulfur/$cm^2$) are necessitated to push the energy density of Li−S battery beyond the current lithium-ion battery.[22−24]

Graphene, a two-dimensional honeycomb $sp^2$ carbon lattice, has received worldwide attention for its potential application in next-generation energy storage devices due to its intriguing electrical and chemical properties.[7,34−37] Nitrogen-doped graphene, combining the advantages of graphene and nitrogen-doped carbon, is an ideal nanoscale building block to construct a high-sulfur-content nitrogen-doped carbon host for Li−S batteries. However, graphene sheets tend to form irreversible agglomerates or even restack to form graphite through van der Waals interactions during all phases of graphene preparation and subsequent electrode production, resulting in the loss of specific surface area.[38−42] This will lower the polysulfides adsorption capacity due to decrease of the accessible active sites located on the surface of graphene.[42] Although the advances have been made in the pursuit of nitrogen-doped graphene as sulfur host for Li−S batteries recently,[27,43,44] the electrochemical performance such as the cycling stability and sulfur utilization is still unsatisfied. This indicates that preventing graphene aggregation to maintain the accessible active surface and constructing adequate pore volume to host sulfur are of particular importance when graphene sheets are used as electrode materials for Li−S batteries.

Herein, we report a highly crumpled nitrogen-doped graphene (NG) sheet as sulfur host for Li−S battery. Numerous wrinkles endow NG an ultrahigh pore volume (5.4 $cm^3/g$) and large surface area (1158 $m^2/g$), which enable strong polysulfide adsorption and high sulfur content in the NG host. As expected, the nitrogen-doped graphene sheet-sulfur (NG-S) cathode shows a high capacity of 1227 mAh/g and long cycle life (75% capacity retention after 300 cycles) at high sulfur content of 80 wt %. A high capacity of 1082 mAh/g is still achieved with an ultrahigh sulfur content of 90 wt %, and a capacity of 832 mAh/g is retained after 200 cycles. Thanks to the high capacity and high sulfur loading, an areal capacity of 5 mAh/$cm^2$ was achieved on the electrode level at such high sulfur content.

The highly crumpled nitrogen doped-graphene sheets were synthesized through a facile thermally induced expansion approach with cyanamide serving as both nitrogen source and porogen and thus eliminating the need for other templates commonly used. The synthesis process is schematically shown in Figure 1, panel a, in which graphene oxide (GO) made by a modified Hummer's method was used a precursor, and cyanamide served as nitrogen source and porogen (see details in Supporting Information). Nitrogen adsorption−desorption isotherms (Figure 1b) show a type-IV isotherm curve with H1 hysteresis, indicating the presence of mesopores. The narrowness of the hysteresis loops with steep and nearly parallel adsorption and desorption branches reveal that the NG particles have good pore connectivity, and the corresponding Brunauer−Emmett−Teller (BET) specific surface area and Barrett−Joyner−Halenda (BJH) pore volume are 1158 $m^2/g$ and 5.4 $cm^3/g$, respectively. The BJH pore size distribution (Figure S1) shows that the NG possesses hierarchical pore structures with the pore size ranging from 2−50 nm.



DOI: 10.1021/acs.nanolett.5b03217
Nano Lett. 2016, 16, 864−870

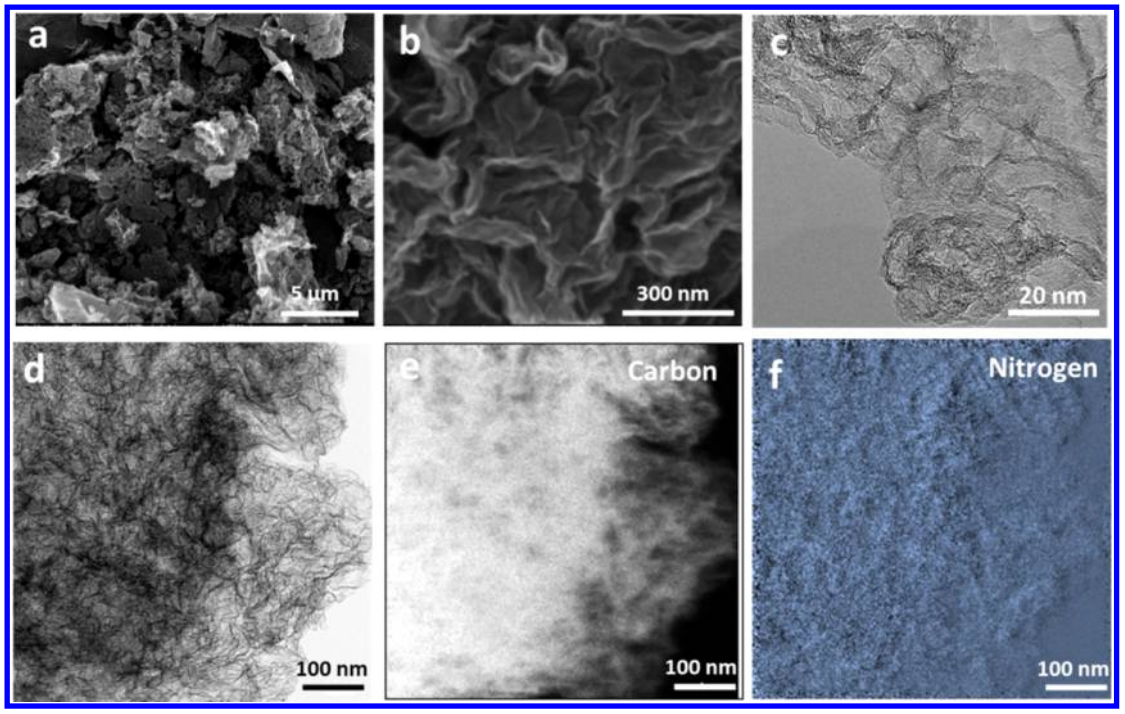


**Figure 2.** (a) Lo- and (b) high-magnification SEM images, and (c) high-resolution TEM image of the highly crumpled NG sheets; (d) energy filtered TEM image and corresponding EELS elemental mapping of the highly crumpled NG sheets: (e) carbon and (f) nitrogen.

Although several approaches, including chemical vapor deposition (CVD), solvent thermal, and $N_2H_4$ treatment, have been developed, the synthesis of large-pore-volume (>4 $cm^3/g$) NG is still lacking.[45] In this study, we used cyanimide, as both swelling agent and nitrogen-doping source, to be directly reduced to nitrogen-based analogues under 5% $H_2$/Ar atomosphere in the following heat treatment process. It is different from previous method using cyanimide precursor with the carbon nitride ($C_3N_4$) intermediate formed under pure argon flow gas.[46] The selection of the flow gas and optimization of heat treatment process have an important impact on the pore volume and surface area of NG sheets. The NG sheets synthesized under pure argon flow gas show a pore volume of 3.5 $cm^3/g$ only (Figure 1b), consistent with previous findings.[46,47] To clarify mechanism of the NG formation process with these two flow gas, the GO−cyanamide composites, treated at 600 °C under Ar and $H_2$ (5%)/Ar separately, were collected and analyzed by Fourier transform infrared spectroscopy (FT-IR) (Figure S2) and X-ray photoelectron spectroscopy (XPS, Figure S3). As to the NG intermediate with $H_2$/Ar atmosphere, disappearance of the characteristic triazine peak at 825 $cm^{-1}$ in the FT-IR spectra indicates absence in formation of $C_3N_4$.[48] Instead, the peaks at 1640 and 1322 $cm^{-1}$ assigned to C═N and N−H bond of pyrrolic and pyridinic groups in nitrogen-doped carbon were clearly observed.[49] This is further supported by the observation of corresponding $N_{1S}$ peak in the deconvoluted XPS profiles of the NG intermediate with $H_2$/Ar atmosphere (Figure S3). We thus found that the NG−cyanimide precursor undergoes a different pathway under two different flow gases. This is mainly because the nitrogen-containing species of GO−cyanimide precursor, such as HC≡NH-$NH_2$, can be reduced under $H_2$ reduction gas. Once reduced, this species cannot further form carbon nitride ($C_3N_4$) because of disappearance of the -C≡NH group that is necessary for the self-condensation reaction for the synthesis of carbon nitride. We further monitored the surface area and pore volume of the NG materials under Ar/$H_2$ atmosphere at different stages and found that they are increasing during the carbonization process (Figure S4 and Table S2), indicating a continuous pore forming and nitrogen-doping process. The pore volume reaches as high as 5.4 $cm^3/g$ when the temperature increased to 900 °C. As discussed in the earlier part, large pore volume is vital for high-energy-density Li−S batteries that necessitate high sulfur content in the electrode. A pore volume at least of 2.94 $cm^3/g$ is required for porous carbon to accommodate 80 wt % sulfur and is dramatically increased to 4.94 $cm^3/g$ when 90 wt % sulfur content is made. The ultrahigh pore volume of the highly crumpled NG sheets affords the possibility to achieve 90 wt % sulfur content in NG-S composite and thus makes the high-energy-density Li−S battery feasible.

XPS showed the presence of C, N, and O atoms at the NG sheet surface (Figure 1c). The binding energy peaks observed in the high-resolution N 1s profile at 397.8 and 400.5 eV can be attributed to pyridinic and pyrrolic nitrogen, respectively.[50] The highly crumpled NG sheets include 6.53 wt % nitrogen determined by elemental analysis. The structure of the crumbled NG sheets is further investigated by the Raman spectroscopy (Figure 1d). The spectrum shows a weak D band (1360 $cm^{-1}$) and strong G band (1580 $cm^{-1}$); the D band corresponds to the defects and disorder in the structure of the graphene sheets due to the nitrogen-doping, while the G band is related to the $E_{2g}$ vibration of $sp^2$ C atoms in graphene.

The morphology of the highly crumpled NG sheets was examined by electron microscopy. Scanning electron microscopy (SEM) images (Figure 2a,b) confirm that the NG sheets display a fluffy and corrugated morphology with more wrinkles and folded regions compared to GO−cyanamide (Figure S5). These crumpled NG sheets randomly aggregate with each other to form a disordered solid (Figure 2a). NG sheets are highly crumpled but maintain their two-dimensional (2D) sheet structure as shown in the energy filtered transmission electron



DOI: 10.1021/acs.nanolett.5b03217
*Nano Lett.* 2016, 16, 864−870

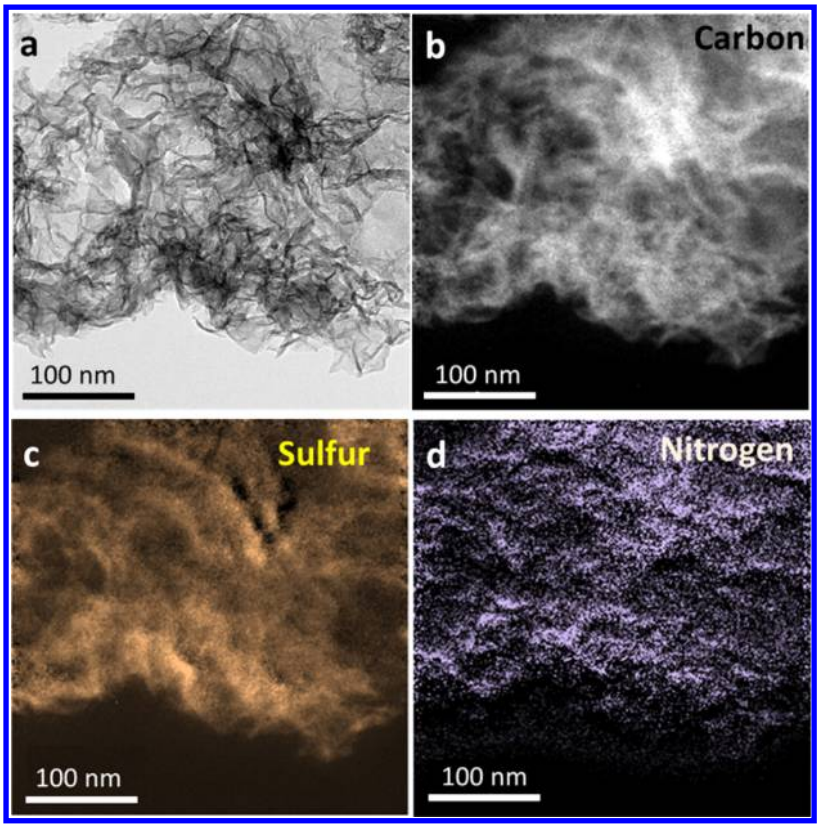


**Figure 3.** (a) EF-TEM image and corresponding EELS elemental mapping of (b) carbon, (c) sulfur, and (d) nitrogen for NG-S90 composite with 90 wt % sulfur content.

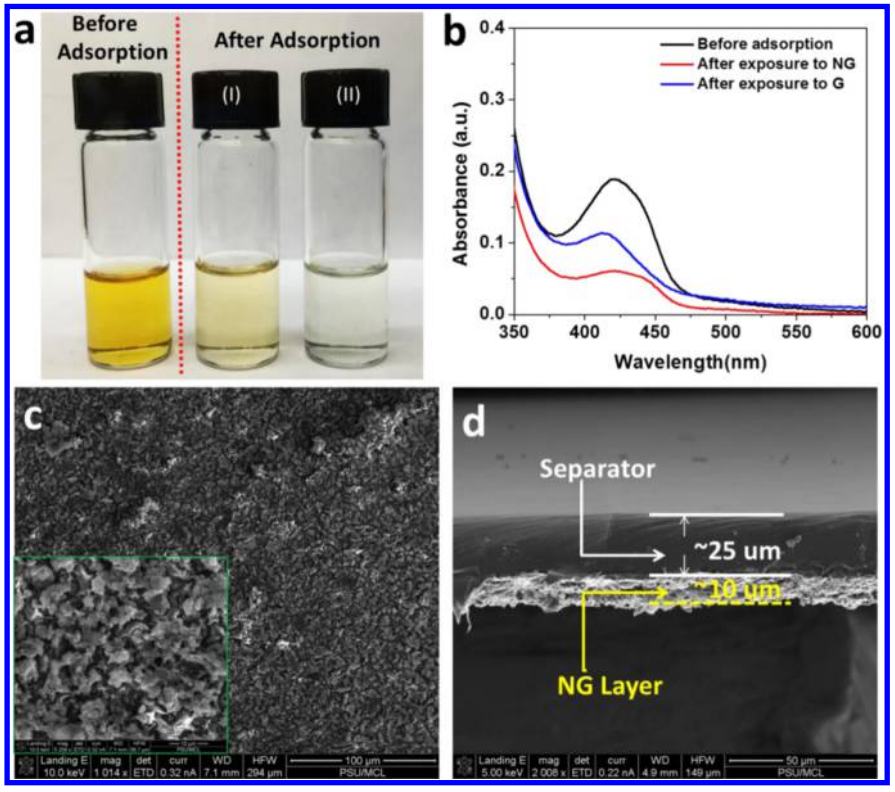


**Figure 4.** (a) Photograph and (b) UV−vis spectra of the polysulfide solution after exposure to the different adsorbers: (I) undoped graphene sheets, (II) highly crumpled nitrogen-doped graphene sheets; (c) low- and high-magnification (inset) SEM images (top view) of the NG sheet-coated separator; (d) cross-sectional SEM images of the NG sheet-coated separator. The thickness of the NG layer is about 10 $\mu$m, and the areal mass loading is about 0.4 mg/cm$^2$.



DOI: 10.1021/acs.nanolett.5b03217
*Nano Lett.* 2016, 16, 864−870

microscopy (EF-TEM) images (Figure 2d). The high-resolution TEM image (Figure 2c) further reveals that the thin wall typically consists of only a few layers of graphene sheets. Corresponding electron energy loss spectroscopy (EELS) mapping (Figure 2e,f) shows similar intensity across the sample, indicating the uniform distribution of nitrogen in the sample. The crumpling of the graphene sheets can significantly prevent them from agglomerating and restacking with one another thus increasing the electrolyte-accessible surface area, which is reflected by the high BET surface area and pore volume of the NG sheets shown in Figure 1, panel b.

The NG-S nanocomposites were prepared by a melt-diffusion method (see details in Supporting Information). The resultant composite is denoted as NG-SX, where X is the weight percentage of sulfur in the composite. The sulfur content in the composite was confirmed by thermogravimetric analysis (Figure S6 in Supporting Information). High sulfur content up to 90 wt % in the composite is possible due to the ultrahigh pore volume and nitrogen-doping-induced chemisorption. The pore volume and surface area in NG-S composites remarkably decreased after sulfur loading (Figure S7 in Supporting Information), confirming that sulfur flowed into the pores of the highly crumpled NG sheets. The chemical adsorption of sulfur on the carbon likely allowed the sulfur to be uniformly distributed within the framework. The EF-TEM images and corresponding EELS elemental mappings of carbon, nitrogen, and sulfur of NG-S90 composite are shown in Figure 3. All three mapping images were found to have similar intensity across the sample, suggesting a uniform distribution of sulfur in the composites.

We further evaluated adsorption ability of the as-synthesized highly crumpled NG sheets on lithium polysulfides using an ex situ adsorption measurement. Typically, lithium polysulfides with an overall stoichiometric ratio matching $Li_2S_8$ in THF solution were investigated using ultraviolet−visible (UV−vis) spectroscopy before and after exposure to NG sheets and undoped graphene (single/double layered graphene, ACS Materials Co.), as shown in Figure 4, panels a and b. Strong absorbance in the 400−500 $cm^{-1}$ region is clearly observed for fresh polysulfide solution, which is consistent with the literature.[51,52] Polysulfide solutions exposed to both the nitrogen-doped and undoped graphene showed lower absorbance in this region, indicating adsorption of polysulfides by the graphene materials, but the absorbance for the solution exposed to NG was significantly lower of the solution exposed to undoped graphene (Figure 4b). This strongly suggests that the nitrogen-doping can remarkably enhance the adsorption of lithium polysulfides, which coincides with our recent findings.[25] This is further confirmed by the lighter color of the polysulfides solution after exposure to NG sheets (Figure 4a). The NG sheets can thus effectively trap soluble polysulfides during cycling, mitigating loss of active materials. Since adsorption sites are embedded within the highly conductive carbon matrix, electrochemical redox of the polysulfides can take place while they are adsorbed. In addition, the strong chemical adsorption can promote more even deposition of solid sulfur and $Li_2S$, preventing active material loss by formation of large, inactive particles.[24,25] These factors make the highly conductive, strongly adsorbing nitrogen-doped graphene an excellent choice for a Li−S battery cathode framework.

Recent studies have shown that insertion of a carbon interlayer between the cathode and separator can both significantly decrease the resistance of the sulfur cathode and enhance active material utilization by trapping the soluble lithium polysulfides within the carbon interlayer.[53,54] Strong adsorption ability makes the highly crumbled NG sheet an ideal material for fabricating such an interlayer. To this end, the NG sheet was coated on separator (Celgrad 2325) using PVDF as the binder (Figure 4c). The thickness of the NG sheet layer was controlled at around 10 $\mu$m (Figure 4d), and the mass loading was around 0.4 mg/$cm^2$. The control of thin and light coating layer can minimize the adverse effect of decrease of the sulfur content (see calculation in Supporting Information). The large pore volume of NG sheets also allows it accommodate the large amount of sulfur when used a cathode framework as discussed in the previous section. To fully utilize the NG sheet materials, Li−S cells with NG-S composite cathodes materials and NG-coated separators as interlayer were fabricated and tested.

The battery performance of the NG sheets-based cells was studied in two-electrode CR2016 coin cells with lithium metal as the counter electrode. Figure 5, panels a and b show a typical cyclic voltammogram (CV) and a discharge−charge profile of an NG-based cell at a current density of 0.39 mA/$cm^2$ between 1.9 and 3.0 V, respectively. The discharge curve shows two plateaus at around 2.3 and 2.1 V versus $Li/Li^+$, corresponding to the reduction of sulfur to higher order lithium polysulfides ($Li_2S_n$, $6 \leq n \leq 8$) and the reduction of higher-order lithium polysulfides to lower-order lithium polysulfides ($Li_2S_n$, $2 \leq n < 6$) and $Li_2S$, respectively.[6] The reverse reactions, corresponding to the oxidation of low-order polysulfides and high-order polysulfides, are indicated by the two plateaus in the charge curve, which resemble the redox peaks in CV scanning. In addition, no major polarization was observed in the voltage profile of NG-based cells despite such high sulfur content in the cathodes. The cycle life and Coulombic efficiency of the NG sheet-based cells with NG-S80 and NG-S90 cathodes are shown in Figure 5, panel c. The high sulfur content and low fractions of carbon black additive and polymer binder allow the sulfur content in the electrode to 72 wt % (72 wt % sulfur in the electrode = 90 wt % sulfur in the NG-S composite × 80 wt % NG-S composite in the electrode). The overall sulfur content in both carbon−sulfur composite (90 wt %) and electrode (72 wt %) in our study is much higher than that in most previous publications.[7,14,17,26,55] High sulfur content is essential for enhancing the energy density of the cells, as it lowers the inactive materials fraction and thereby enhances the cell gravimetric energy density. A high initial capacity of 1227 mAh/g was attained at 0.39 mA/$cm^2$ when using NG-S80 cathodes, corresponding to 77% sulfur utilization even with such a high sulfur content. The NG-based cells show excellent cycle stability in the following 300 cycles at a higher current density of 1.17 mA/$cm^2$ with capacity retention of 75%. The loss of only 0.08% capacity loss per cycle at such high sulfur content is outstanding compared to the existing literature. Surprisingly, even when increasing the sulfur content to 90 wt %, a high capacity of 1082 mAh/g was still obtained in the first cycle. Although this is slightly lower than with NG-S80 cathodes, a high capacity of 833 mAh/g was still observed after 200 cycles.

When considering practical applications, achieving high areal capacity is critical, as it increases the ratio of active to inactive materials in the cell. The areal capacity of the electrode is calculated as specific capacity (mAh/g) of sulfur × sulfur mass loading (g sulfur/$cm^2$ of electrode face area). A high sulfur loading is thus necessary for reaching a high areal capacity. However, specific capacity is often very dependent on the sulfur



DOI: 10.1021/acs.nanolett.5b03217
Nano Lett. 2016, 16, 864−870

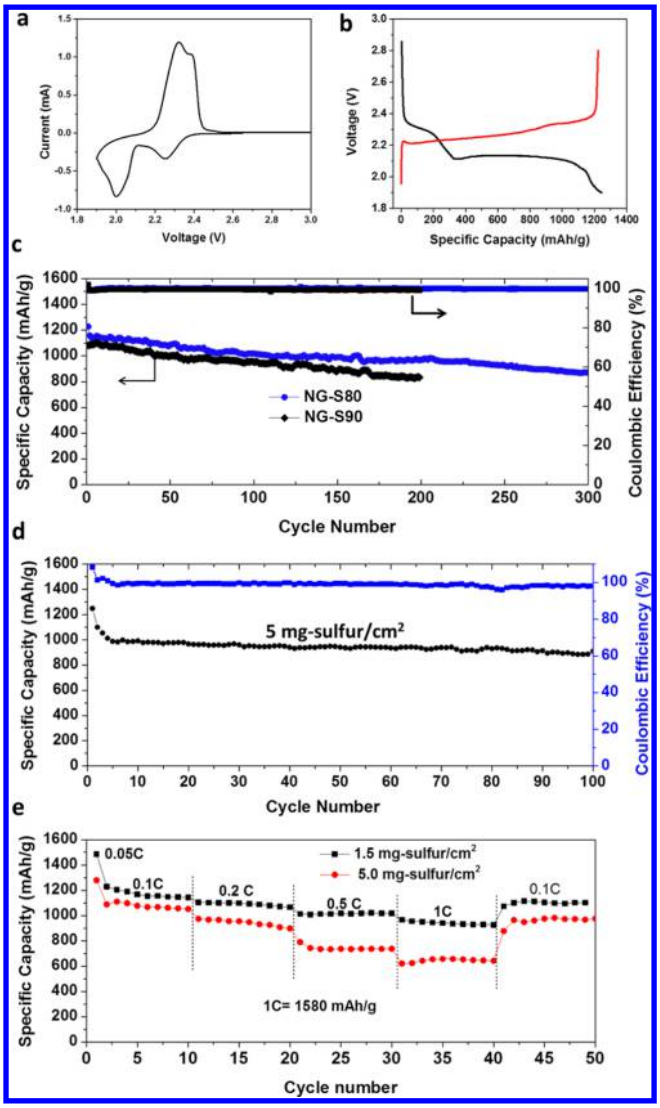


**Figure 5.** (a) Typical CV curves and (b) discharge−charge voltage-capacity profile of the cells with NG-S80 cathodes and NG sheet-coated separators; (c) cycling stability and Coulombic efficiency of NG-based cells with NG-S80 and NG-S90 cathodes at a current density of 0.39 mA/cm$^2$ for the first cycles and 1.17 mA/cm$^2$ for the subsequent cycles. The sulfur loading for the NG-S80 and NG-S90 cathodes is ∼1.5 mg-sulfur/cm$^2$; (d) cycling stability and Coulombic efficiency of the NG-based cells with NG-S80 cathodes with a high sulfur loading of 5 mg-sulfur/cm$^2$ at a current density of 0.45 mA/cm$^2$ for the first cycles and 1.3 mA/cm$^2$ for the subsequent cycles; (e) the rate capability of NG-based cells with NG-S80 cathode at different sulfur loading. All capacity values were calculated based on the mass of sulfur.

loading and will drop with increasing sulfur loading due to the increased electrical resistance of the electrode.[56] The high sulfur content and the large particle size of the NG-S composite allow electrodes with a high mass loading of above 5 mg sulfur/cm$^2$ to be fabricated, which is a key factor for reaching high cell-level gravimetric/volumetric energy density based on total cell weight or volume. The sulfur loading in this study is around 2.5−10-times higher than in most other nanostructured carbon−sulfur electrodes (0.5−2 mg/cm$^2$).[7,14,17,55] The high sulfur utilization, good excellent cycle stability, and high Coulombic efficiency at high sulfur loading and high current make the NG-based cells more attractive for high-energy-density Li−S battery.

The rate capability of NG-based cells was further evaluated as shown in Figure 5, panel e. For the NG-S80 cathode with 1.5 mg-sulfur/cm$^2$, a specific capacity of 1486 mAh g$^{-1}$, ∼1160 mAh g$^{-1}$, ∼1100 mAh g$^{-1}$, and ∼1000 mAh g$^{-1}$ was obtained at 0.05C, 0.1C, 0.2C, and 0.5C, respectively. Even at 1C, the NG-S80 cathode still can deliver a high reversible capacity of ∼950 mAh g$^{-1}$. When the rate was restored to 0.1C after 40 cycles of rate testing, the specific capacity of the NG-S80 cathode returned to ∼1120 mAh g$^{-1}$, close to the 1160 mAh g$^{-1}$ from the initial 0.1C trial. This indicates that the cathode charge/discharge was reversible even at high current density. With further increasing sulfur loading to 5 mg sulfur/cm$^2$, the NG-S80 cathode presents a relatively low capacity than that in 1.5 mg sulfur/cm$^2$ at the same current density. The decrease of the capacity for high-loading electrode is due to the increased ohmic resistance. The NG-S80 cathode still shows a high capacity of ∼930 mAh/g, 730 mAh/g, and 650 mAh/g at 0.2C, 0.5C, and 1C, respectively. This result is a significant progress toward the high-sulfur content, high sulfur loading cathode for Li−S battery, and the rate performance is also outstanding compared with the existing literature.[57]

In summary, we demonstrated synthesis of highly crumpled nitrogen-doped graphene sheets through a facile thermally induced expansion approach in which the cyanamide was used as both nitrogen resource and porogen simultaneously. The as-prepared highly crumpled nitrogen-doped graphene sheets exhibit an ultrahigh pore volume of 5.4 cm$^3$/g along with a high surface area of 1158 m$^2$/g. Cells using this nitrogen-doped graphene sheet, used as both a sulfur host for Li−S battery and a cathode-protecting interlayer material, show high capacity and long-cycle life even at high sulfur contents up to 90%. In addition, a high areal capacity of ∼5 mAh/cm$^2$ was demonstrated at a high sulfur loading of 5 mg sulfur/cm$^2$ and high sulfur content of 80 wt %. This excellent performance is due to unique characteristics of the highly crumpled nitrogen-doped graphene particles: high pore volume, unstacked graphene layers, and strong lithium polysulfides adsorption. This material thus presents a promising path for further development in Li−S batteries and can be potentially exploited for other applications such as supercapacitors and oxygen reduction reaction catalysts.

## ■ ASSOCIATED CONTENT

### Supporting Information

The Supporting Information is available free of charge on the ACS Publications website at DOI: 10.1021/acs.nanolett.5b03217.

Experimental section; calculation of maximum sulfur content in porous materials and sulfur content in the NG-based cells; $N_{1S}$ XPS spectra, FTIR spectra, and TEM studies of GO-cyanamide composite; TGA curves of NG-S80 and NG-S90 composites; $N_2$ sorption isotherms of NG-S90 composite; rate capability of NG-based Li−S cells (PDF)

## ■ AUTHOR INFORMATION

### Corresponding Author

*E-mail: dwang@psu.edu.

### Notes

The authors declare no competing financial interest.



DOI: 10.1021/acs.nanolett.5b03217
*Nano Lett.* 2016, 16, 864−870

## ■ ACKNOWLEDGMENTS

This work was supported by the Assistant Secretary for Energy Efficiency and Renewable Energy, Office of Vehicle Technologies of the U.S. Department of Energy under Contract No. DE-EE0005475.

## ■ REFERENCES

(1) Bruce, P. G.; Freunberger, S. A.; Hardwick, L. J.; Tarascon, J.-M. *Nat. Mater.* **2011**, *11*, 19−29.
(2) Yang, Y.; Zheng, G.; Cui, Y. *Chem. Soc. Rev.* **2013**, *42*, 3018−32.
(3) Manthiram, A.; Fu, Y.; Su, Y.-S. *Acc. Chem. Res.* **2013**, *46*, 1125−1134.
(4) Zhang, C.; Wu, H. B.; Yuan, C.; Guo, Z.; Lou, X. W. *Angew. Chem., Int. Ed.* **2012**, *51*, 9592−5.
(5) Weng, W.; Pol, V. G.; Amine, K. *Adv. Mater.* **2013**, *25*, 1608−1615.
(6) Ji, L.; Rao, M.; Zheng, H.; Zhang, L.; Li, Y.; Duan, W.; Guo, J.; Cairns, E. J.; Zhang, Y. *J. Am. Chem. Soc.* **2011**, *133*, 18522−18525.
(7) Wang, H.; Yang, Y.; Liang, Y.; Robinson, J. T.; Li, Y.; Jackson, A.; Cui, Y.; Dai, H. *Nano Lett.* **2011**, *11*, 2644−2647.
(8) Liu, J.; Li, W.; Duan, L.; Li, X.; Ji, L.; Geng, Z.; Huang, K.; Lu, L.; Zhou, L.; Liu, Z.; Chen, W.; Liu, L.; Feng, S.; Zhang, Y. *Nano Lett.* **2015**, *15*, 5137−42.
(9) Ai, G.; Dai, Y.; Ye, Y.; Mao, W.; Wang, Z.; Zhao, H.; Chen, Y.; Zhu, J.; Fu, Y.; Battaglia, V.; Guo, J.; Srinivasan, V.; Liu, G. *Nano Energy* **2015**, *16*, 28−37.
(10) Chen, H.; Wang, C.; Dai, Y.; Qiu, S.; Yang, J.; Lu, W.; Chen, L. *Nano Lett.* **2015**, *15*, 5443−8.
(11) Han, X.; Xu, Y.; Chen, X.; Chen, Y.-C.; Weadock, N.; Wan, J.; Zhu, H.; Liu, Y.; Li, H.; Rubloff, G.; Wang, C.; Hu, L. *Nano Energy* **2013**, *2*, 1197−1206.
(12) Zhou, W.; Xiao, X.; Cai, M.; Yang, L. *Nano Lett.* **2014**, *14*, 5250−6.
(13) Huang, J.-Q.; Zhang, Q.; Peng, H.-J.; Liu, X.-Y.; Qian, W.-Z.; Wei, F. *Energy Environ. Sci.* **2014**, *7*, 347−353.
(14) Ji, X.; Lee, K. T.; Nazar, L. F. *Nat. Mater.* **2009**, *8*, 500−506.
(15) Jayaprakash, N.; Shen, J.; Moganty, S. S.; Corona, A.; Archer, L. A. *Angew. Chem., Int. Ed.* **2011**, *50*, 5904−5908.
(16) Schuster, J.; He, G.; Mandlmeier, B.; Yim, T.; Lee, K. T.; Bein, T.; Nazar, L. F. *Angew. Chem., Int. Ed.* **2012**, *51*, 3591−3595.
(17) Xin, S.; Gu, L.; Zhao, N.-H.; Yin, Y.-X.; Zhou, L.-J.; Guo, Y.-G.; Wan, L.-J. *J. Am. Chem. Soc.* **2012**, *134*, 18510−18513.
(18) Liang, C. D.; Dudney, N. J.; Howe, J. Y. *Chem. Mater.* **2009**, *21*, 4724−4730.
(19) Guo, J.; Xu, Y.; Wang, C. *Nano Lett.* **2011**, *11*, 4288−4294.
(20) Dorfler, S.; Hagen, M.; Althues, H.; Tubke, J.; Kaskel, S.; Hoffmann, M. J. *Chem. Commun. (Cambridge, U. K.)* **2012**, *48*, 4097−4099.
(21) Peng, H.-J.; Huang, J.-Q.; Zhao, M.-Q.; Zhang, Q.; Cheng, X.-B.; Liu, X.-Y.; Qian, W.-Z.; Wei, F. *Adv. Funct. Mater.* **2014**, *24*, 2772−2781.
(22) Zhang, S. S. *J. Power Sources* **2013**, *231*, 153−162.
(23) Xu, T.; Song, J.; Gordin, M. L.; Sohn, H.; Yu, Z.; Chen, S.; Wang, D. *ACS Appl. Mater. Interfaces* **2013**, *5*, 11355−11362.
(24) Song, J.; Xu, T.; Gordin, M. L.; Zhu, P.; Lv, D.; Jiang, Y.-B.; Chen, Y.; Duan, Y.; Wang, D. *Adv. Funct. Mater.* **2014**, *24*, 1243−1250.
(25) Song, J.; Gordin, M. L.; Xu, T.; Chen, S.; Yu, Z.; Sohn, H.; Lu, J.; Ren, Y.; Duan, Y.; Wang, D. *Angew. Chem., Int. Ed.* **2015**, *54*, 4325−4329.
(26) Qiu, Y.; Li, W.; Zhao, W.; Li, G.; Hou, Y.; Liu, M.; Zhou, L.; Ye, F.; Li, H.; Wei, Z.; Yang, S.; Duan, W.; Ye, Y.; Guo, J.; Zhang, Y. *Nano Lett.* **2014**, *14*, 4821−4827.
(27) Wang, X.; Zhang, Z.; Qu, Y.; Lai, Y.; Li, J. *J. Power Sources* **2014**, *256*, 361−368.
(28) Wang, C.; Su, K.; Wan, W.; Guo, H.; Zhou, H.; Chen, J.; Zhang, X.; Huang, Y. *J. Mater. Chem. A* **2014**, *2*, 5018−5023.
(29) Tang, C.; Zhang, Q.; Zhao, M.-Q.; Huang, J.-Q.; Cheng, X.-B.; Tian, G.-L.; Peng, H.-J.; Wei, F. *Adv. Mater.* **2014**, *26*, 6100−6105.
(30) Ji, X.; Evers, S.; Black, R.; Nazar, L. F. *Nat. Commun.* **2011**, *2*, 325.
(31) Choi, Y. J.; Jung, B. S.; Lee, D. J.; Jeong, J. H.; Kim, K. W.; Ahn, H. J.; Cho, K. K.; Gu, H. B. *Phys. Scr.* **2007**, *T129*, 62−65.
(32) Zhang, Y.; Wang, L.; Zhang, A.; Song, Y.; Li, X.; Feng, H.; Wu, X.; Du, P. *Solid State Ionics* **2010**, *181*, 835−838.
(33) Seh, Z. W.; Zhang, Q.; Li, W.; Zheng, G.; Yao, H.; Cui, Y. *Chem. Sci.* **2013**, *4*, 3673−3677.
(34) Raccichini, R.; Varzi, A.; Passerini, S.; Scrosati, B. *Nat. Mater.* **2014**, *14*, 271−279.
(35) Liu, J. *Nat. Nanotechnol.* **2014**, *9*, 739−741.
(36) Wu, H.; Kong, D.; Ruan, Z.; Hsu, P.-C.; Wang, S.; Yu, Z.; Carney, T. J.; Hu, L.; Fan, S.; Cui, Y. *Nat. Nanotechnol.* **2013**, *8*, 421−425.
(37) Xu, Y.; Bai, H.; Lu, G.; Li, C.; Shi, G. *J. Am. Chem. Soc.* **2008**, *130*, 5856−5857.
(38) Xiao, L.; Damien, J.; Luo, J.; Jang, H. D.; Huang, J.; He, Z. *J. Power Sources* **2012**, *208*, 187−192.
(39) Jiang, L.; Fan, Z. *Nanoscale* **2014**, *6*, 1922−1945.
(40) Liu, G.; Wang, Y.; Xu, C.; Qiu, F.; An, C.; Li, L.; Jiao, L.; Yuan, H. *Nanoscale* **2013**, *5*, 1074−1081.
(41) Zang, J.; Ryu, S.; Pugno, N.; Wang, Q.; Tu, Q.; Buehler, M. J.; Zhao, X. *Nat. Mater.* **2013**, *12*, 321−325.
(42) Cranford, S. W.; Buehler, M. J. *Phys. Rev. B: Condens. Matter Mater. Phys.* **2011**, *84*, 205451.
(43) Qiu, Y.; Li, W.; Zhao, W.; Li, G.; Hou, Y.; Liu, M.; Zhou, L.; Ye, F.; Li, H.; Wei, Z.; Yang, S.; Duan, W.; Ye, Y.; Guo, J.; Zhang, Y. *Nano Lett.* **2014**, *14*, 4821−7.
(44) Wang, C.; Su, K.; Wan, W.; Guo, H.; Zhou, H.; Chen, J.; Zhang, X.; Huang, Y. *J. Mater. Chem. A* **2014**, *2*, 5018.
(45) Wang, H.; Maiyalagan, T.; Wang, X. *ACS Catal.* **2012**, *2*, 781−794.
(46) Wen, Z.; Wang, X.; Mao, S.; Bo, Z.; Kim, H.; Cui, S.; Lu, G.; Feng, X.; Chen, J. *Adv. Mater.* **2012**, *24*, 5610−5616.
(47) Hong, J.; Xia, X.; Wang, Y.; Xu, R. *J. Mater. Chem.* **2012**, *22*, 15006−15012.
(48) Sanni, S. O.; Idemudia, O. G. *J. Nanomater.* **2015**, *2015*, 8.
(49) Zheng, F.; Yang, Y.; Chen, Q. *Nat. Commun.* **2014**, *5*, 5261.
(50) Pels, J. R.; Kapteijn, F.; Moulijn, J. A.; Zhu, Q.; Thomas, K. M. *Carbon* **1995**, *33*, 1641−1653.
(51) Barchasz, C.; Molton, F.; Duboc, C.; Leprêtre, J.-C.; Patoux, S.; Alloin, F. *Anal. Chem.* **2012**, *84*, 3973−3980.
(52) Patel, M. U. M.; Demir-Cakan, R.; Morcrette, M.; Tarascon, J.-M.; Gaberscek, M.; Dominko, R. *ChemSusChem* **2013**, *6*, 1177−1181.
(53) Zhou, G.; Pei, S.; Li, L.; Wang, D. W.; Wang, S.; Huang, K.; Yin, L. C.; Li, F.; Cheng, H. M. *Adv. Mater.* **2014**, *26*, 664.
(54) Su, Y.-S.; Manthiram, A. *Nat. Commun.* **2012**, *3*, 1166.
(55) Lee, Y. M.; Choi, N.-S.; Park, J. H.; Park, J.-K. *J. Power Sources* **2003**, *119*−*121*, 964−972.
(56) Lv, D.; Zheng, J.; Li, Q.; Xie, X.; Ferrara, S.; Nie, Z.; Mehdi, L. B.; Browning, N. D.; Zhang, J.-G.; Graff, G. L.; Liu, J.; Xiao, J. *Adv. Energy Mater.* **2015**, *5*, 1402290.
(57) Qie, L.; Manthiram, A. *Adv. Mater.* **2015**, *27*, 1694−700.



DOI: 10.1021/acs.nanolett.5b03217
*Nano Lett.* 2016, 16, 864−870